NPS-61-83-008

NAVAL POSTGRADUATE SCHOOL

Monterey, California

UNIPOLAR ARCING, A BASIC
LASER DAMAGE MECHANISM

F. Schwirzke

05 May 1983

Approved for public release; distribution unlimited

Prepared for:
Chief of Naval Research, Arlington, VA 22217 and
Naval Research Laboratory, Washington, DC 20375

FedDocs
D 208.14/2
NPS-61-83-008

D 208.14/2:
NPS-01-83-006

NAVAL POSTGRADUATE SCHOOL
Monterey, California

Rear Admiral J. J. Ekelund
Superintendent

David A. Schrady
Provost

The work reported herein was supported in part with funds provided by the Naval Postgraduate School Foundation Research Program and in part the by Naval Research Laboratory, Washington, DC through work request N00173245000.

Reproduction of all or part of this report is authorized.

This report was prepared by:

DUDLEY KNOX LIBRARY
NAVAL POSTGRADUATE SCHOOL
MONTEREY CA 93943-5101

UNCLASSIFIED

SECURITY CLASSIFICATION OF THIS PAGE (When Data Entered)

REPORT DOCUMENTATION PAGE

READ INSTRUCTIONS BEFORE COMPLETING FORM

1. REPORT NUMBER: NPS-61-83-008	2. GOVT ACCESSION NO.
3. RECIPIENT'S CATALOG NUMBER	
4. TITLE (and Subtitle): Unipolar Arcing, A Basic Laser Damage Mechanism	5. TYPE OF REPORT & PERIOD COVERED: Technical Report
6. PERFORMING ORG. REPORT NUMBER	
7. AUTHOR(s): F. Schwirzke	8. CONTRACT OR GRANT NUMBER(s)
9. PERFORMING ORGANIZATION NAME AND ADDRESS: Naval Postgraduate School, Monterey, CA 93940	10. PROGRAM ELEMENT, PROJECT, TASK AREA & WORK UNIT NUMBERS: 62761N; WF61-544-000 N0017382WR20159
11. CONTROLLING OFFICE NAME AND ADDRESS: Chief of Naval Research, Arlington, VA 22217; Naval Research Laboratory, Washington, DC 20375	12. REPORT DATE: May 1983
	13. NUMBER OF PAGES: 21
14. MONITORING AGENCY NAME & ADDRESS(If different from Controlling Office)	15. SECURITY CLASS. (of this report): UNCLASSIFIED
	15a. DECLASSIFICATION/DOWNGRADING SCHEDULE

16. DISTRIBUTION STATEMENT (of this Report)

Approved for public release; distribution unlimited.

17. DISTRIBUTION STATEMENT (of the abstract entered in Block 20, if different from Report)

18. SUPPLEMENTARY NOTES

This report is a reprint of a paper which was presented at the Fourteenth Annual Symposium on Optical Materials for High Power Lasers, November 16-17, 1982, National Bureau of Standards, Boulder, CO.

19. KEY WORDS (Continue on reverse side if necessary and identify by block number)

Damage mechanism
Laser-induced unipolar arcing
Unipolar Arc Model

20. ABSTRACT (Continue on reverse side if necessary and identify by block number) Unipolar arcing has been shown to be the primary plasma-surface interaction process when a laser produced plasma is in contact with a surface. Evidence of unipolar arcing was found on all targets irradiated at atmospheric pressure that also arced in vacuum, stainless steel, titanium, molybdenum, copper, and aluminum. Cratering was observed even for a defocused and low-power laser pulse. The minimum laser power density required for the onset of breakdown on the surface is also sufficient to cause arc damage. Never was there a plasma evident without attendant unipolar arc craters.

DD FORM 1 JAN 73 1473 EDITION OF 1 NOV 65 IS OBSOLETE
S/N 0102-014-6601

UNCLASSIFIED

SECURITY CLASSIFICATION OF THIS PAGE (When Data Entered)

About 500,000 arc craters per cm^2 have been observed on laser illuminated metal surfaces although no external voltage is applied. Smaller size craters with a density of about $10^8/cm^2$ have been found on higher resistivity materials. The higher resistivity requires the radially inward surface return current to converge to a smaller cathode spot size to achieve sufficient power density to vaporize and ionize the material required for running the unipolar arc. The local increase of the plasma pressure above the cathode spot leads to an electric field configuration which drives the arc current and also facilitates the return current flow to the surface and cathode spot. Unipolar arcing concentrates the available laser-plasma energy towards the cathode spot. Large scale unipolar arcing on metal surfaces increases the coupling of energy from the laser heated plasma into the target. The ejection of a plasma jet from the cathode crater also causes highly localized shock waves to propagate into the target, softening it in the process. Thus, material erosion is much more severe than it would be case for uniform energy deposition over a larger area. This research has wide spread applications. Any situation in which a sufficiently hot surface plasma exists there will be unipolar micro-arcing. The physics relates to other forms of electrical breakdown on surfaces and electrodes.

UNIPOLAR ARCING, A BASIC LASER DAMAGE MECHANISM

F. Schwirzke

Naval Postgraduate School
Monterey, California 93940

Laser beams interact with surfaces by a variety of thermal, impulse and electrical effects. Energy coupling is considerably enhanced once surface electrical breakdown occurs. The laser heated plasma interacts then with the surface via three major interrelated damage mechanisms: thermal evaporation, ion sputtering, and unipolar arcing. While the first two are purely thermal and mechanical effects, unipolar arcing is an electrical plasma-surface interaction process which leads to crater formation, usually called laser-pitting, a process which was often observed but not well understood. Without any external voltage applied, many electrical micro-arcs burn between the surface and the laser heated plasma, driven by local variations of the sheath potential with the surface acting as both the cathode and anode. Unipolar arcing represents the most damaging and non-uniform laser-plasma-surface interaction process since the energy available in the plasma concentrates towards the cathode spots. This causes cratering of the surface. Unipolar arcing is the primary plasma-surface interaction process once breakdown occurs. The onset of arc damage is coincident with the onset of plasma formation. Never was there a plasma evident without attendant unipolar arc craters. At low irradiance there was no other laser damage (like melting) observed, all damage was in the form of unipolar arc damage.

Key Words: Laser damage mechanism; Laser-induced unipolar arcing; Unipolar arc model.

1. INTRODUCTION

Progress in pulsed power technology has been hampered by many plasma physics and technical problems not the least of which has been the problem area of plasma surface interactions. Surface breakdown by high power laser radiation leads to the formation of a plasma layer in front of the laser illuminated surface. Unipolar arcing then occurs at a sufficiently high plasma electron temperature.

The term unipolar arc was first used by Robson and Thoneman [1] in 1958. In their article they described the existence of an arc which "required only one electrode and is maintained by the thermal energy of the plasma electrons." The basis of their model is that at equilibrium there must be zero net current between an exposed conducting plate and a plasma. A retarding potential is established between plate and plasma. This floating sheath potential V_f prevents all but the higher energy electrons in the maxwellian distribution to reach the surface. Thus at equilibrium the net current becomes zero. The sheath potential depends on the electron temperature. If the electron temperature, T_e, is sufficiently large such that V_f exceeds the potential to initiate and sustain an arc, the authors argued that there will be strong local emission of electrons from a cathode spot on the plate into the plasma. Figure 1 represents this process. The plasma potential then lowers from V_f to the cathode fall potential V_c of the arc. With the plasma potential now lowered more electrons can return to the plate, thus closing the current loop and maintaining the plasma's quasi-neutrality. The circulating current is given by the increased

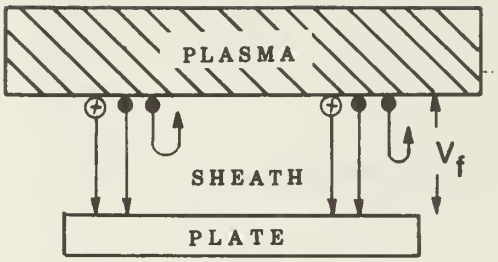

Figure 1a. Equilibrium flow of electrons and ions to isolated plate.

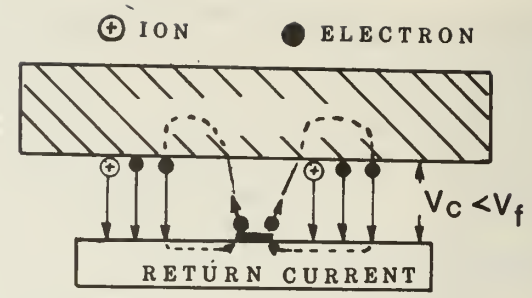

Figure 1b. Equilibrium flow of electrons and ions to isolated plate with electron emission from a cathode spot.

electron return current to the plate of area A due to the reduction of the sheath potential from V_f to V_c,

$$I_c = Aen_e \left[\frac{(kT_e)}{(2\pi m_e)}\right]^{1/2} \left\{ \exp\left(\frac{-eV_c}{kT_e}\right) - \exp\left(\frac{-eV_f}{kT_e}\right)\right\} \qquad (1)$$

n_e is the electron density, k the Boltzmann constant and e the elementary charge. The arc was sustained, they argued, until I_c fell below a minimum current I_a. The value of I_a depends on the material of the plate. The Robson-Thoneman mechanism implies a constant plasma electron density n_e contributing to the return current over a large area A of the wall.

The existence of unipolar arcs has been verified with extensive experimental evidence. Arc tracks have been observed on many tokamak surfaces [2-6].

2. UNIPOLAR ARC MODEL

While the Robson-Thoneman mechanism describes essentially the return current flow by eq (1), our model elaborates upon the electric fields which are set up in the plasma and drive the arc. The condition of plasma quasi-neutrality, $n_e = n_i$, leads to the formation of a sheath wherever the plasma is in contact with a wall. Since the electrons have a higher thermal velocity than the ions, an ion rich boundary layer is formed and the plasma potential is positive with respect to the wall. The magnitude of this sheath- or floating-potential is proportional to T_e, depends weakly on the ion/electron mass ratio M_i/m_e, and is independent of the plasma density,

$$V_f = (kT_e/2e)\ell n(M_i/2\pi m_e) \qquad (2)$$

The sheath width is proportional to the Debye shielding length

$$\lambda_D = (kT_e/4\pi n_e e^2)^{1/2} \qquad (3)$$

The plasma loss rate to the wall is controlled by the sheath potential. It accelerates the ions and electrostatically reflects most of the electrons

such that electrons and ions reach the surface in equal numbers. Since the ions are much more effective than electrons in the desorption and sputtering of surface particles and the rates increase steeply with energy in the range of interest, sputtering and desorption of loosely bound particles [7] become worse if the sheath potential increases due to an increase of the electron temperature near the wall [8]. Electron and ion recombination on the surface contribute to surface heating.

Unipolar arcing, where the wall acts as both the anode and the cathode, occurs if the sheath potential increases sufficiently to ignite and sustain an arc. The Robson-Thoneman unipolar arc model implies a constant plasma density. However, for an arc to develop it is also necessary that the ion density increases above the cathode spot, in order to enable a larger electron current to flow into the plasma. Figure 2 shows schematically our unipolar arc model which takes into account the increase of plasma density due to ionization of neutrals released from the cathode spot.

The initial experiments were conducted on type 304 stainless steel targets [9] which had been highly polished. Surface protrusions, metallurgical inhomogenities, inclusions or whiskers from processing operations such as milling and grinding can serve as initial cathode spots. Furthermore, plasma waves and associated potential fluctuations in the sheath [10] can enhance electron emission and initiate cathode spots. The increased electric field strength on surface protrusions will also increase the ion flux from the plasma to these spots. Increased ion bombardment and recombination rates lead to a locally increased surface temperature. This results in desorption of neutral gas molecules and evaporation of metal atoms from the surface spot into the plasma. The ionization of a small fraction of the released neutral atoms results in a local increase in density of the plasma above the cathode spot.

The equation of motion for the electron fluid is given by

$$\rho_e \frac{\partial \vec{V}_e}{\partial t} = -en_e(\vec{E} + \vec{V}_e \times \vec{B}) - \nabla P_e + \frac{n_e e}{\sigma} \vec{j} = 0 \qquad (4)$$

Where $\rho_e = n_e m_e$ is the electron mass density, $\vec{V}_e$ the fluid velocity of the electrons, P_e the pressure, j the current density, and σ the electrical conductivity. The electron inertial term is insignificant for the characteristic time for arc evolution. Thus, setting eq (4) equal to zero and furthermore for B = 0, solving for E, one obtains,

$$\vec{E} = \frac{\vec{j}}{\sigma} - \frac{1}{n_e e} \nabla P_e$$

For j = 0, the ambipolar electric field becomes $E_o = -(1/e\ n_e)\nabla P_e$

For a weakly ionized plasma, the ratio $j/\sigma = \Delta E$ becomes independent of n_e and small in comparison to E_o:

$$\Delta E = \frac{j}{\sigma} = \frac{n_e e V_e (m_e \nu)}{(n_e e^2 \lambda_e)} = \frac{m_e V_e \nu}{e\lambda_e} < E_o = -\frac{\nabla P_e}{n_e e} \approx \frac{kT_e}{ed} \approx \frac{m_e}{2} \frac{\bar{v}^2}{ed}$$

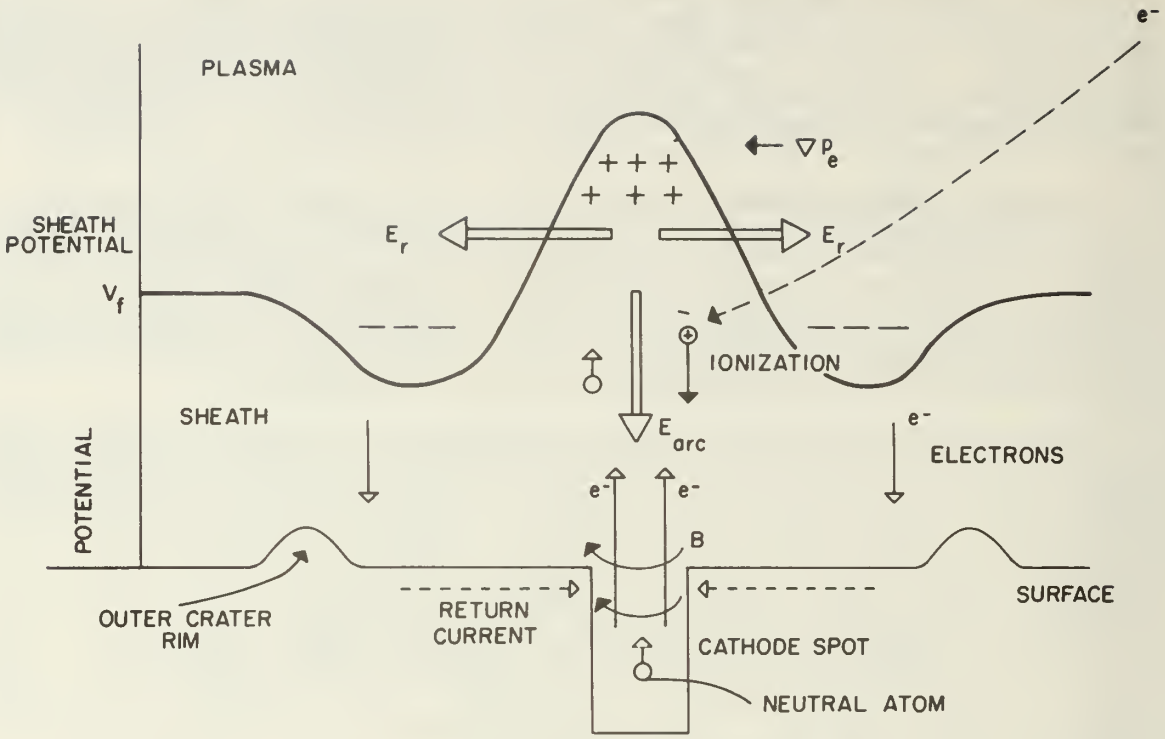

Figure 2. Unipolar arc model

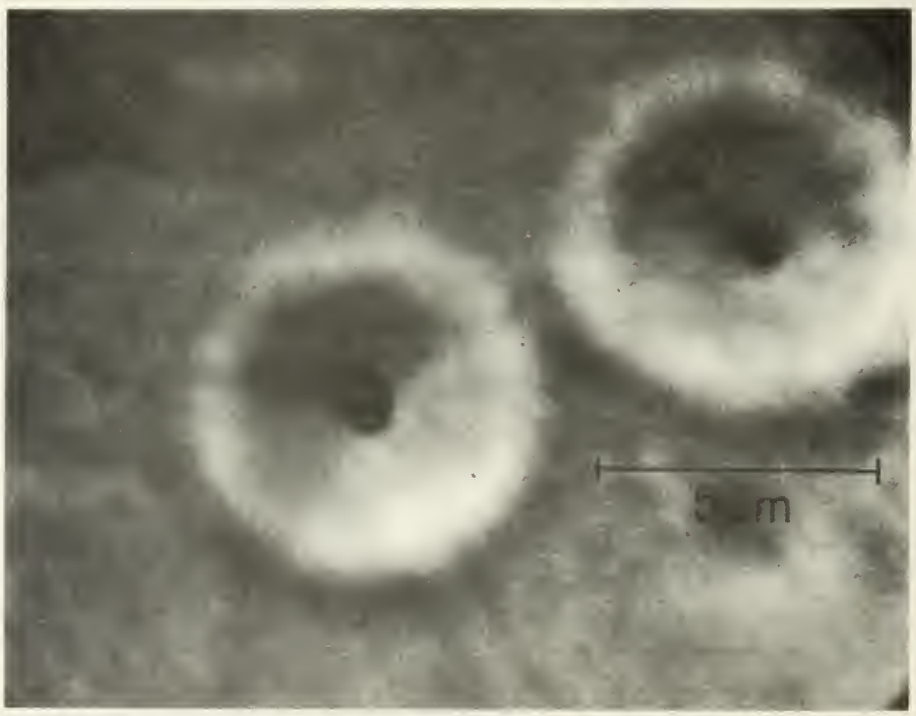

Figure 3. Unipolar arc craters. The outer rim diameter is 5.5 μm. The dark cathode spot at the center has a diameter of 0.7 μm, smaller than the laser wavelength of λ = 1.06 μm.

Our model implies that the mean free path length λ_e is larger than the dimensions of the neutral cloud above the cathode spot. Since the build-up of the plasma pressure gradient is caused by ionizing a fraction of the neutral particles, we assume $\lambda_e > d$, where d is the characteristic pressure gradient length. Even if $\lambda_e \lesssim d, E < E_o$ since the current associated drift velocity of the electrons $V_e << v$, where v is the electron thermal velocity.

The probability that a neutral atom is ionized in or near the sheath is of the order of the Debye length divided by the mean free path length. This ratio is much less than unity. For values of $n_e = 5 \times 10^{14}$ cm^{-3} and kT = 10eV, which may be representative for an initial laser produced low density plasma layer, $\lambda_D = 10^{-4}$ cm. The electron mean free path for ionizing a neutral atom is $\lambda_e = 1/n_o\sigma_i$. Under vacuum conditions the neutral particle density n_o in the sheath depends on the desorption and evaporation rates from the surface. Iron atoms emitted at the melting temperature of 1526°C leave the surface with a thermal velocity of about 10^5 cm s^{-1}. Their time of flight to pass through the sheath would be 10^{-9} s. If, for example only one monolayer, i.e., 2×10^{15} particles cm^{-2} are released from a surface spot during this time, the neutral particle density within a Debye length will increase to $n_o = 2 \times 10^{19}$ cm^{-3}. (For comparison, atmospheric density at 0°C corresponds to 2.7×10^{19} cm^{-3}.) If we assume that the ionization cross section σ_i is 10^{-17}cm^2, λ_e becomes 0.005 cm. Thus a small fraction, $\lambda_D/\lambda_e = 2 \times 10^{-2}$, of the neutral atoms would be ionized within a Debye length from the surface. This, however, increases the plasma density from 5×10^{14} cm^{-3} to $n_i = (2 \times 10^{-2})\, n_o = 4 \times 10^{17}$ cm^{-3}, i.e., by a factor of 800 within 1 ns. Correspondingly, the local λ_D would rapidly decrease to 3.7×10^{-6} cm.

An ion produced in the sheath is driven back to the surface by the electric field which is of the order

$$E \approx V_f/\lambda_D \qquad (5)$$

The time of flight to return to the surface is proportional to the Debye length and the acceleration in the electric field $a = (eV_f)/(M_i\lambda_D)$. Thus

$$t = (2\lambda_D/a)^{1/2} = \lambda_D(2M_i/eV_f)^{1/2}$$

For the initially assumed Debye length of 10^{-4} cm an iron ion needs about 10ps to fall back to the surface. Since the Debye length decreases with build-up of the local plasma density above the cathode spot, later released neutrals which become ionized in the sheath need only picoseconds to return to the surface. The increased ion bombardment and release of recombination energy lead to a further increase in surface temperature. This in turn represents a feedback mechanism, leading to a further release of absorbed gases and material evaporation at a sufficiently high power deposition. Since the mean free path for electrons is much larger than the sheath width, the additional ionization of neutral atoms in (or near) the sheath and the acceleration of these ions in the sheath implies a concentration of available plasma energy towards the arc spot. Of course, most of the neutral atoms released from the surface become ionized within the plasma. The locally increased plasma density reduces λ_D and thus the sheath width. Correspondingly, the locally increased plasma pressure above the cathode spot leads to an increasing electric field E_{arc}(V/cm) to drive the arc current:

$$|E_{arc}| \approx V_c/\lambda_D \lesssim V_f/\lambda_D = 6.6 \times 10^{-3}(n_e\, kT_e)^{1/2} \qquad (6)$$

where kT_e is measured in electronvolts and n_e in reciprocal cubic centimeters. The high density plasma above the cathode spot is biased with respect to the surface via the cathode fall potential of the arc. The high density plasma dominates the surrounding lower density background plasma. The increased plasma pressure above the cathode spot thus also leads to an

electric field E_r in the radial direction, tangential to the surface:

$$E_r = - \frac{kT_e}{en_e} \frac{dn_e}{dr} + \frac{j}{\sigma} \tag{7}$$

Neglecting the j/σ term, this radial field reduces the plasma potential in a ring-like area surrounding the higher plasma pressure above the arc spot by

$$\Delta V(r) = \frac{kT_e}{e} \ell n \frac{n_e(r)}{n_{eo}} \tag{8}$$

The ratio of the maximum plasma density above the cathode spot to the unperturbed plasma density can easily be of the order $(n_e/n_{eo}) \sim 10^3$ or larger. The reduced sheath potential in this ring area allows more electrons from the high energy tail in the maxwellian distribution to reach the surface, this closing the current loop of the unipolar arc, figure 2. In fact, equating ΔV with the sheath's floating potential, eq (2)

$$\Delta V = V_f$$

$$\frac{kT_e}{e} \ell n \frac{n_e}{n_{eo}} = \frac{kT_e}{2e} \ell n \frac{Mi}{2\pi m_e}$$

we find that independent of the electron temperature the sheath potential approaches zero when

$$\frac{n_e}{n_{eo}} = \left(\frac{Mi}{2\pi m_e} \right)^{1/2}$$

In this case, the electron return current to the surface is determined by n_e and the electron thermal velocity. This electron saturation current is

$$i_s^- = \frac{en_e v}{4} A \tag{9}$$

Equation (9) can be used to estimate the order of magnitude of the surface area A needed for the electron return current. If the arc current is 10 Amp and $n_e = (M_i/2\pi m_e)^{1/2} n_{eo} = 130 n_{eo}$ for the mass M_i of iron ions and if we consider a laser produced plasma near the surface with initially $n_{eo} = 5 \times 10^{14}$ cm^{-3} and $kT_e = 10$ eV, the return current area is $A = \pi r^2 = 3 \times 10^{-9}$ m^2. Actually, $n_e(r)$ will rapidly increase above the assumed value, reducing A further. Thus the estimated value of the radius of $r \lesssim 30$ μm is of the same order as the radius of the outer crater rim. The location of the outer crater rim thus may indicate how far the return current area has expanded during the limited burntime of the arc.

3. EXPERIMENT

A plasma generated by a neodymium laser pulse was used to study unipolar arcing on solid material surfaces. A Korad K-1500 laser was operated in the Q-switched mode. Nominal beam pulse half width of the laser was 25 ns. Incident laser energy was varied by inserting neutral density filters of varying transmittance in the beam path. For low energy shots the laser amplifier was not fired. Laser energies on target between 0.0075 and 10 joules were obtained by these techniques. The beam was focused to various spot sizes on the target to provide further variation in power density at the target. Laser energy at each shot was measured using a Laser Precision RK-3200 Pyroelectric Energy Meter, with a RE 549 detector reading via an 8% splitter in the main beam.

The laser pulse was directed onto targets placed in a vacuum chamber. The vacuum system using an oil diffusion pump and a liquid nitrogen cooled baffle, was capable of providing chamber pressures of the order 10^{-6} Torr. To obtain a smooth surface the target disks were metallographically polished with a final polishing slurry of 0.05 μm Al_2O_3. Before being mounted in the test chamber, each specimen was cleaned with acetone. After one laser shot the damage on the polished surface was observed with an optical and a scanning electron microscope, Cambridge Stereoscan S4-10.

4. LASER-INDUCED UNIPOLAR ARCING

Laser induced unipolar arcing was studied over a wide range between two extreme, basically different laser-power and plasma-dynamic conditions on various metals and nonconducting surfaces.

1. High Irradiance

A high power laser pulse is focused onto the target. The laser produced plasma expands from the small focal spot over the target surface into areas which were not illuminated by the laser. The area damaged by the plasma is much larger than the laser focus area. The existence of unipolar arc craters in these areas proves that unipolar arcing is a plasma-surface interaction process, independent of the laser-plasma interaction processes, like self-focusing, filamentation, instability, etc. The laser just heats the electrons to a sufficiently high temperature.

2. Low Irradiance

A low power, defocused laser pulse is used to determine the laser power density threshold for onset of unipolar arcing. Laser intensity variations over the cross section (hot spots) cause breakdown and arcing only in areas where the power density was sufficiently high. The area damaged by the plasma is smaller than the laser illuminated area.

The high and the low irradiance experiments will be discussed in the following paragraphs and the results on conducting and non-conducting surfaces will be compared.

4.1 High Irradiance Laser Induced Arcing

In the Q-switched mode the range of energies on the target was selected as 3-5J, giving a power range of 100-200 MW. The laser focal spot diameter is approximately 0.5 mm. For a 200 MW pulse this gives a typical power density of 10^{11} W cm^{-2}. The temperature of the laser-produced plasma was measured spectroscopically, $kT_e \approx 100eV$. Time of flight measurements showed that the plasma expands rapidly with a velocity of about 10^7 cm/s from the focal spot on the target surface in the normal and radial directions.

The laser impact crater of about 0.75 mm diameter is surrounded by a plasma damaged surface area of about 6 mm diameter. Although no external voltage is applied, about 300,000 to 600,000 unipolar arc craters/cm^2 are observable on the stainless steel surface which was exposed to the radially expanding plasma but not to the laser radiation. Figures 4-6 show

a sequence of SEM photos of the plasma-damaged surface for increasing distance from the laser focal spot. Close in, figure 4 shows a superposition of arc craters. The oldest one, burning for a longer time during the existence of the laser-heated plasma, have larger outer rim diameters of 30-50 μm. Smaller craters within larger ones are probably initiated towards the end of the laser pulse. They have smaller outer rim diameters. If not refilled by the liquid metal, craters show a dark spot of about 1 μm size at the center representing the cathode spot. The size of the outer rim craters also decreases with increasing distance from the focal spot (figures 5 and 6). Figure 6 shows the onset of crater formation near the edge of the expanding plasma.

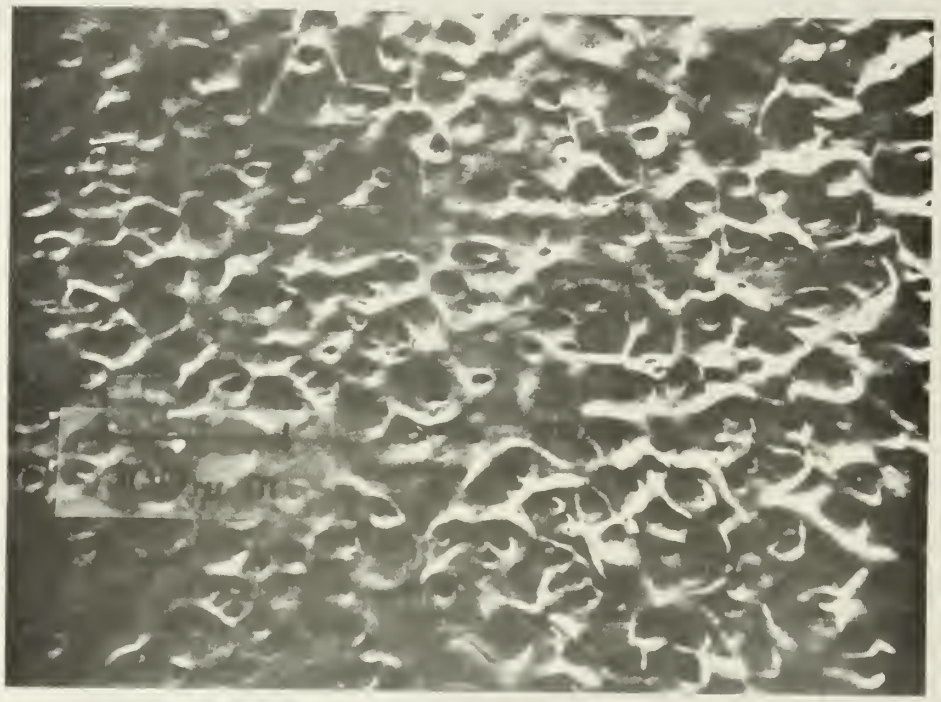

Figure 4. Overlapping craters near laser focal spot. Outer rim crater size depends on arc burn time.

Figure 5. Crater formation at 1.5mm from laser focal spot which is located beyond the left side.

Figure 6. Onset of unipolar arc crater formation on highly polished stainless steel.

Deep cathode craters of 0.5 to 1 μm diameter are clearly visible with outer crater rim formation just barely beginning. The depth of these fully developed cathode craters is 3-6 μm.

The short lifetime of the laser-produced plasma allows the study of the temporal development of the arcs. The initial breakdown phase of unipolar arcing is documented by the small but deep cathode craters formed furthest away from the focal spot, figure 6, where the plasma conditions favorably for arc formations lasted only for a short time because after laser shut off T_e decreases rapidly in the expanding plasma. Further in, if allowed to burn long enough, the surface metal area A needed for the electron return current melts. The liquid is pushed outwards in the radial direction by the expanding dense plasma and an outer crater rim of 5-50 μm diameter is formed depending on the arc duration.

The depth of the initial arc crater of 3-6 μm, is larger than the dia-

meter of 1 μm. This indicates that the pinch magnetic field of 40,000 Gauss for a current of 10A and r = 0.5 μm contributes to the concentration of the arc energy onto the small cathode spot, see figures 2 and 3. If kTe = 10eV, this field can confine a plasma with a density up to 4 x 10^{18} cm^2. At this density the Debye length $\lambda_D = 10^{-6} << 1$ μm and it is justified to assume that a high density plasma exists in the arc hole. This represents a hollow cathode configuration and the ionization rate should be high. The depth of the cathode spot craters corresponds to a removal of 10^4 to 10^5 monolayers.

Arcing continues only as long as the laser pulse is heating the electrons for 50-60 ns. The natural life time of a micro-arc seems to be of the order of 10 ns. Unipolar arcing on different materials has been studied. All metals show a very similar kind of arc craters. Evidence of unipolar arcing has been found on all targets irradiated at atmospheric pressure, that also arced in vacuum indicating that the metal vapor pressure near the surface is of the order or even larger than the atmospheric pressure.

4.2 Determination of Low Irradiance Threshold for Onset of Arcing

The incident laser power density for the onset of arcing was determined for type 304 stainless steel and type 2024 aluminum [11]. Since the energy output is more easily controlled by the introduction of filters than by adjusting laser power supply voltage, the incident power on the target was controlled in this manner. A polaroid camera was positioned above the target to note plasma formation by recording the attendant light. The beam spot size was measured by placing exposed polaroid film at the target position within the vacuum chamber and conducting a series of laser shots to find the average spot size area.

Using this experimental arrangement a series of laser shots were made to determine the power density threshold for breakdown and plasma formation and the power density threshold for unipolar arc formation. Surface breakdown and the formation of a visible plasma layer occur at a laser power density of about 10 MW/cm^2. Unipolar arcing has been shown to be then the primary plasma-surface interaction process once plasma formation occurs. Figures 7 and 8 provide a comparison of the extent of damage between 25.5 MW/cm^2 and 5.4 MW/cm^2. Figure 9, an enlargement of figure 8, shows the minimal damage observed at 5.4 MW/cm^2. The characteristic shape of unipolar arcs becomes clearly visible in the enlarged photo, a small dark cathode spot at the crater center surrounded by a pronounced rim.

A review of the target damage reveals that the damage was not evenly distributed across the laser illuminated area but rather was concentrated in one quadrant, due to non-uniformity in the laser beam, figures 7 and 8. The locations of the beam's hot spots coincide exactly in shape and location with the observed target damage. Since the area used in calculating power density assumed a uniform distribution of energy, the threshold density reported above can only be accurate as an order of magnitude power density for this particular laser.

The data thus obtained suggest that the power density threshold for the onset of breakdown and for the onset of unipolar arcing are the same. The onset of arc damage is coincident with onset of breakdown and plasma formation. Never was there a plasma evident without attendant unipolar arcs. At low power density there was no other direct laser damage (like melting) observed on the target. In fact, all damage was in the form of arc damage.

Figures 10 and 11 show patterns of micro-arc craters produced on polished stainless steel by an unfocused medium power Q-switched laser pulse. Arcing seems to follow the interference fringes of the laser output as clearly visible near the edge of the laser illuminated area. Breakdown and arcing occur in the regions of constructive interference. The expanding plasma pushes the liquid surface layers to form a rim in the region of destructive interference.

Figure 7. Arc damage on stainless steel, defocused laser pulse of 25.5 MW/cm^2 .

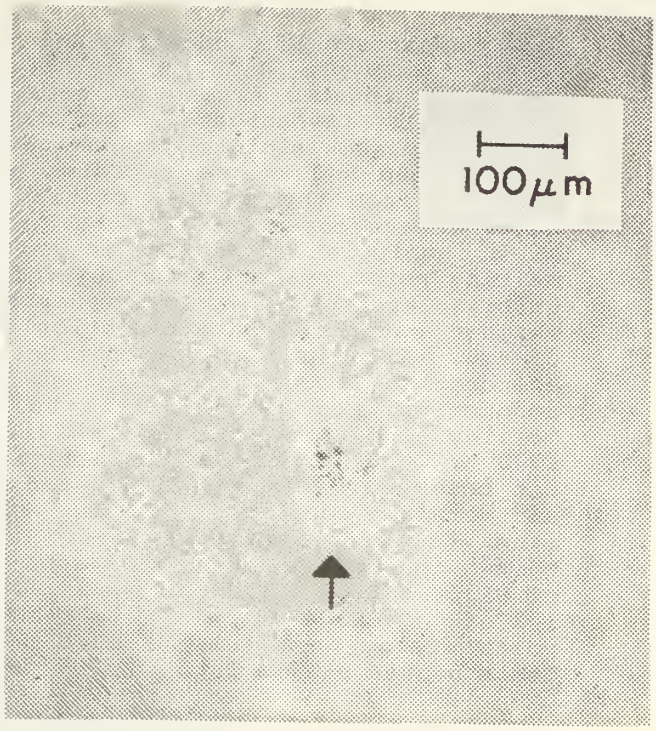

Figure 8. Onset of arcing on stainless steel at 5.4 MW/cm^2 . Same magnification as figure 7.

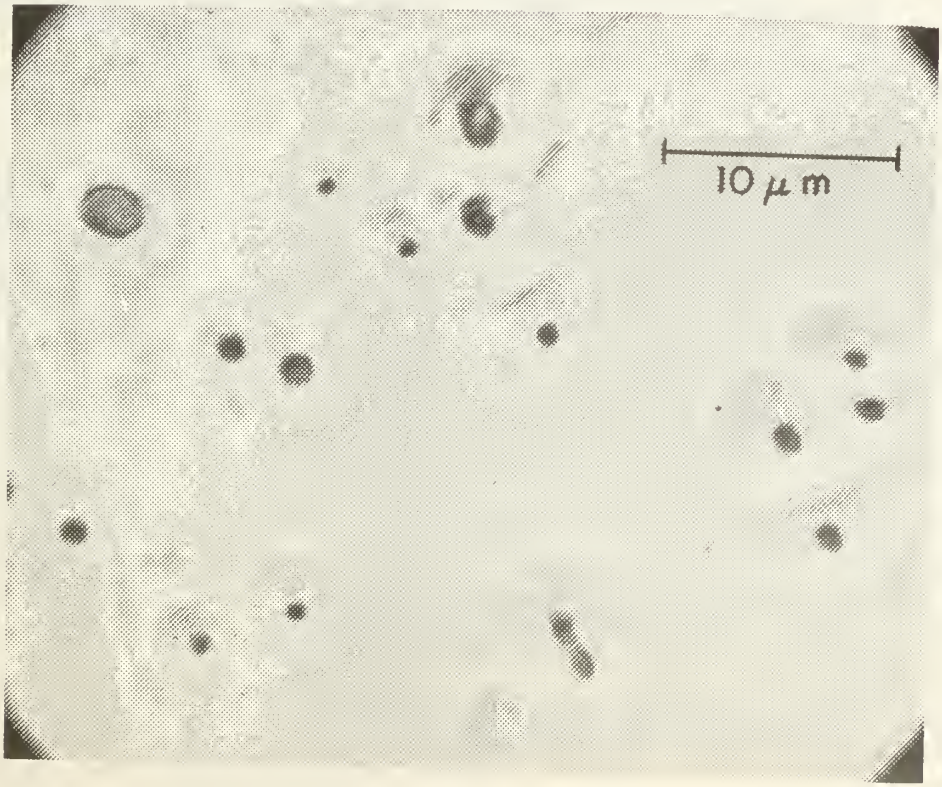

Figure 9. Further magnified view of figure 8. Onset of breakdown and arc formation at 5.4 MW/cm^2.

4.3 Comparison of Conducting and Non-Conducting Surfaces

Laser induced arcing on metal surfaces has been studied extensively. All metals investigated, stainless steel, copper, titanium, aluminum, molybdenum show similar arc damage, a cathode crater of about 1 μm diameter, 3-6 μm deep and an outer crater rim of 5-50 μm diameter. Evaporation of material from the cathode crater and the return current flow through the material are essential for the formation of a unipolar arc. A consequence of our unipolar arc model is that reduced surface conductivity and high melting point materials should influence the arc formation. The effect of unipolar arcing for various types of materials has been studied to determine whether material characteristics have any effect in reducing the arcing damage. Titanium carbide coatings were deposited by an activated reactive evaporation process on stainless steel surfaces. At 20°C the electrical conductivity of TiC is 1/15 the one of SS304, $1.4 \times 10^5 (\text{ohm-cm})^{-1}$. The melting temperature of TiC is 3410 K, roughly twice the value of SS304 at 1770 K. The large size characteristic unipolar arc craters for metals were not observed on laser illuminated TiC coatings [12]. Also, thermal energy and momentum coupling to various target materials was investigated to determine what effect unipolar arcing had on the coupling process [13]. Even though the heat conduction coefficient of TiC is about the same as the one of SS304, a 10 μm TiC coating on SS304 reduced the thermal coupling to about 1/3 of the SS304 value. This leads to the conclusion that large scale unipolar arcing on metal surfaces increases the coupling of energy from the laser heated plasma into the target.

A series of TiC-coated targets was irradiated at power densities ranging from 300 to 1000 MW/cm^2 and the targets were subsequently examined for surface damage. Figure 12 pictures the edge of the damage area. There are regions of apparent melting and resolidification in droplet form, cracking and arcing. Individual arc craters are clearly visible on the right hand side of the figure, in the transition zone to the undamaged area. This indicates again that unipolar arcing is the primary damage mechanism. However, crater sizes are considerably smaller. They range from 0.1 to 0.3 micron diameter, with crater densities of approximately 4.5×10^8 cm^{-2} in regions close to the melted material. Cracking occurs along a narrow band of arc craters, figure 13, indicating that large stress formation is associated with the cratering.

Silicon coatings of 1-2 micron thickness on SS304 and 2024 aluminum were also studied [14]. Figure 14 is a SEM photograph of a 1 micron silicon coating on polished aluminum prior to laser irradiation. This coating shows a bumpy structure. After irradiation at the power density for onset of plasma formation tiny spheres of various degrees of irregularity appear, but the coating does not appear to have melted through. Figure 15 shows the coating near the edge of the laser exposed region. Arc formation starts on the top of the bumps. The crater density is approximately 5×10^7 cm^{-2}, and the crater diameter is about 0.1 micron, again, about 1/10 of the crater size observed on metals.

5. DISCUSSION

The experimental results presented in this paper show that unipolar arcing is the primary laser-plasma-surface interaction mechanism which leads to a very non-uniform energy deposition and crater damage on the surface. Since the scale lengths are very small, typically 1 μm for the cathode spot on metals and the electrons provide the current flow, unipolar arcing should be considered as a fast evolving process with arcs forming within a nanosecond or less.

The initial absorption of laser radiation and plasma heating occur in the underdense plasma close to the surface. The release of material from a cathode spot leads to locally increased absorption of laser radiation and build-up of the plasma pressure until the critical density is reached. Heat conduction by electrons and short wave length plasma radiation provide the energy transport through the overdense plasma to the target surface. Many laser-plasma instabilities have been discussed which may cause non-uniformities near the critical density region. No attention has been

Figure 10. Laser-produced arc pattern near edge of laser illuminated area. Arrows show onset of arcing in ring pattern.

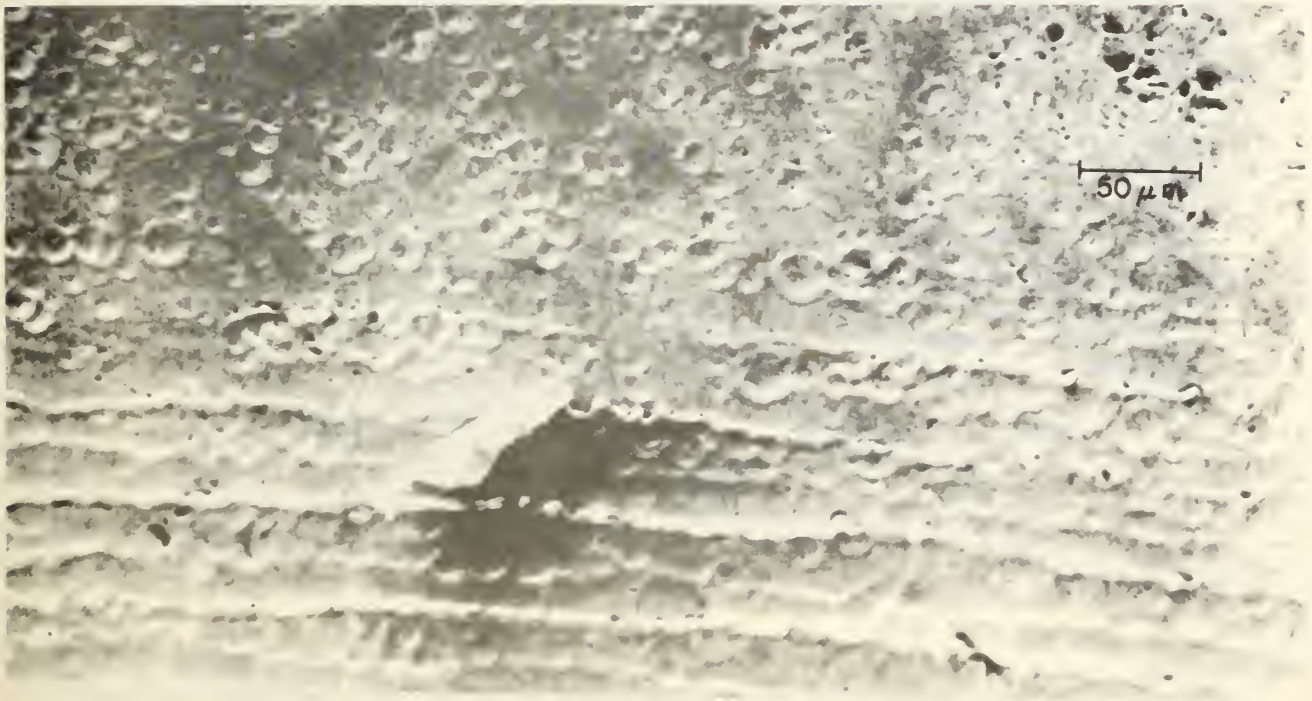

Figure 11. Laser-produced micro-arc pattern on SS304, defocused laser.

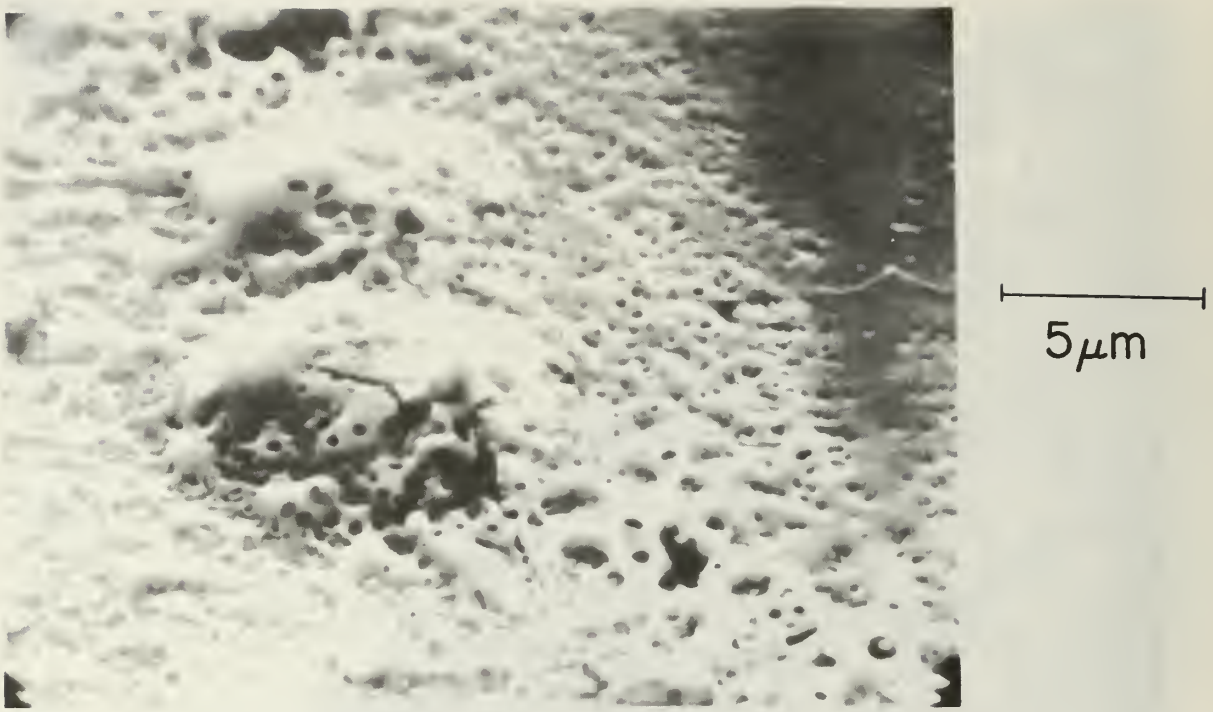

Figure 12. Unipolar arc craters on TiC coated SS304 after irradiation at 300 MW/cm^2.

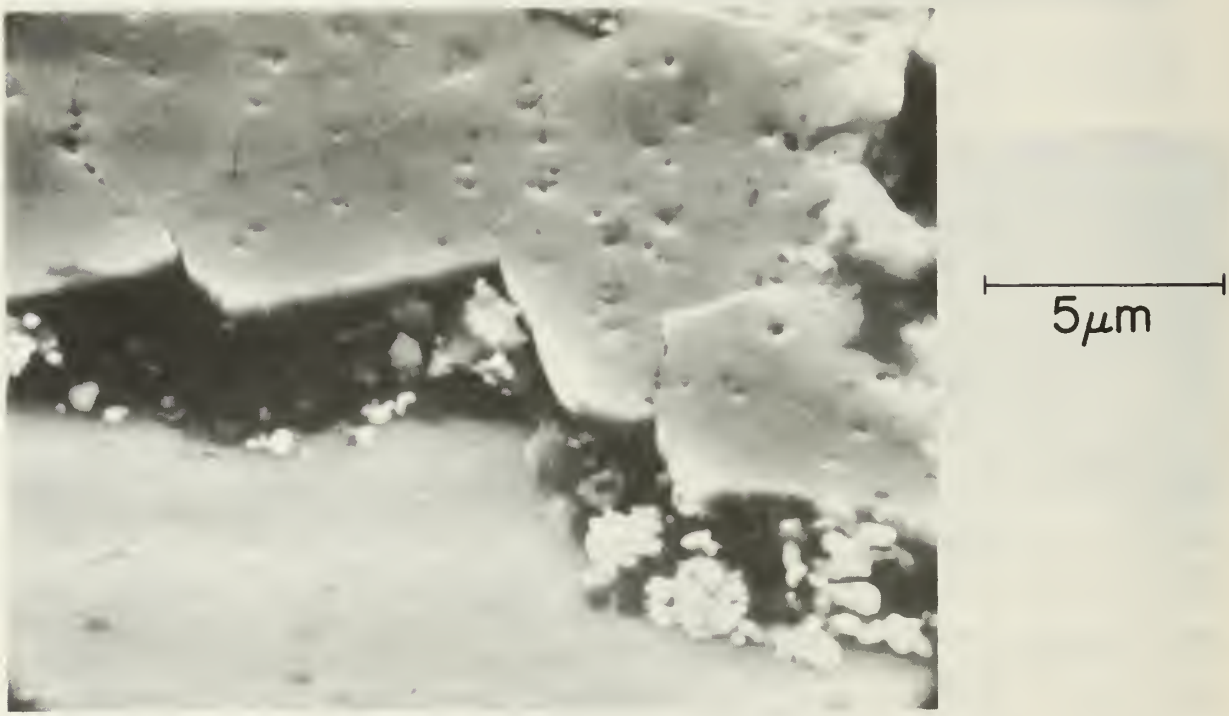

Figure 13. Cracked TiC coating on SS304 after irradiation with 1096 MW/cm^2. The bottom part shows removal of a surface layer. Along the edges of the removed TiC area, cracking follows a narrow band of arc craters.

Figure 14. One micron silicon coating over polished 2024 aluminum before irradiation.

Figure 15. Silicon coating after irradiation with 400 MW/cm^2 near edge of irradiated area.

given to arcing which leads to non-uniform ablation of the material and thus also to a modulation of the critical density contour. The onset of arcing on conducting and non-conducting surfaces will be discussed in the following paragraphs.

5.1 Formation of Low Density Breakdown Plasma

The initial breakdown phase may be characterized by the build up of a low density plasma layer in front of the surface with a density $n_{eo} << n_{ec}$ where n_{ec} is the critical density. This initial plasma layer may be formed by photo electrons and ionization of neutral particles at a distance $\lambda/4$ from the surface where for normal incidence the first maximum in the electric field occurs due to the superposition of the incident wave and the wave reflected on a metal surface. A sheath will form immediately since the sheath potential V_f is independent of the plasma density. The electron temperature might be of the order of 5 to 20eV. Spatial variations of the laser intensity will produce density variations in this initial plasma layer. The electron density can be estimated from the laser produced arc pattern of figure 11. The ring width of about 30 micron is much larger than the laser wave length. The existence of the pattern of this size implies that the local sheath width should be smaller than 30 μm, otherwise the pattern would be "washed out." This assumption $\lambda_D << 30$ μm allows to estimate a lower limit of the plasma density. Assuming again an initial $\lambda_D = 10^{-4}$ cm and T_e = 10eV, we estimate $n_{eo} > 5 \times 10^{14}$ cm^{-3}.

In accordance with eq (6) the sheath electric field increases with the local build up of the plasma pressure as $E \propto p^{1/2}$. The dielectric strength of air at atmospheric pressure is 30 kV/cm. If we take this as a typical value for onset of sparking we find from eq (6) that a plasma layer of only $n_{eo} \geq 2 \times 10^{12}$cm^{-3} and kT_e = 10eV provides already a sheath electric field of $E \geq 30$ kV/cm to start spark formation at atmospheric pressure. As discussed previously, any release of neutral particles from the surface leads to a rapid build up of the local plasma pressure and this further increases the sheath electric field. Thermally enhanced field emission might begin at about 10^6 V/cm, that is at a plasma density of about $n_e = 1.25 \times 10^{17}$cm^{-3}.

Finally, thermionic electron emission from a cathode spot will lead to the formation of an arc. The local build up of the neutral and plasma density then also leads to non-uniform absorption of laser radiation.

5.2 Heating of a Surface Plasma Layer by Laser Radiation

Electrons change momentum through collisions with positive ions and neutral particles. The frictional force acting on the electron fluid is equal to the rate of change of momentum, and the equation of motion for a cold unmagnetized plasma becomes now

$$m_e \frac{\partial \vec{V}_e}{\partial t} = -e\vec{E} - m_e \vec{V}_e \, (\nu_{ei} + \nu_{eo})$$

where ν_{ei} and ν_{eo} are the collision frequencies for momentum transfer due to collisions with ions and neutral particles respectively. The collision frequency in a fully ionized plasma depends on n_i and T_e as

$$\nu_{ei} = 0.29 \times 10^{-6} \, (n_i Z^2 \ell n \Lambda)/(T_e)^{3/2}$$

where T_e is measured in eV and n_i in cm^{-3}, Z is the ionic charge and the Coulomb logarithm is of the order $\ell n \, \Lambda \approx 10$. Electron-neutral collisions dominate for a weakly ionized plasma, $\nu_{ei} << \nu_{eo}$, and ν_{eo} depends on the neutral particle density n_o the collision cross section σ_o (σ_o is of the order 5×10^{-16}cm^2) and the electron thermal velocity

$$\nu_{eo} = n_o \sigma_o v$$

Thus, assuming that ν_{ei} and ν_{eo} are independent of the fluid velocity V_e, we find for an electromagnetic wave of frequency ω for V_e the solution

$$\vec{j} = en_e\vec{V}_e = \frac{n_e e^2}{m_e(\nu_{ei} + \nu_{eo}) + i\omega}\vec{E} = \sigma\vec{E}$$

where the conductivity

$$\sigma = \frac{n_e e^2 \left[(\nu_{ei} + \nu_{eo}) - i\omega\right]}{m_e \left[(\nu_{ei} + \nu_{eo})^2 + \omega^2\right]}$$

The dispersion relation for transverse electromagnetic waves in a plasma can be written as $c^2 = \varepsilon\omega^2/k^2$ with the dielectric constant given by

$$\varepsilon = 1 + \frac{\sigma}{i\omega\varepsilon_o}$$

Thus the dispersion relation becomes

$$k^2c^2 = \omega^2 \left(1 - \frac{\omega_{pe}^2}{(\nu_{ei} + \nu_{eo})^2 + \omega^2} - \frac{i\omega_{pe}^2 (\nu_{ei} + \nu_{eo})}{\omega \left[(\nu_{ei} + \nu_{eo})^2 + \omega^2\right]} \right.$$

where the plasma frequency is defined as $\omega_{pe} = (n_e e^2/m_e\varepsilon_o)^{1/2}$

For the assumed initially weakly ionized plasma layer of $n_e = 5 \times 10^{14}$ cm^{-3} (which is many orders of magnitude below the critical density of $n_{ec} = 10^{21}$ cm^{-3} for Nd laser radiation) and a neutral density layer of $n_o = 2.7 \times 10^{19}$cm^{-3} (which corresponds to atmospheric density at 0°C and 760 Torr), we find $\omega_{pe}^2 << \omega^2$, and $\nu_{ei} << \nu_{eo} \approx 2 \times 10^{12} << \omega$ and eq (10) simplifies to

$$\frac{c^2}{\omega^2/k^2} = \left(1 - \frac{\omega_{pe}^2}{\omega^2}\right) - \frac{i\omega_{pe}^2 \nu_{eo}}{\omega^3} = n^2 = (n_R - in_I)^2 = n_R^2 - n_I^2 - 2in_Rn_I \quad (11)$$

The refractive index $n^2 = \varepsilon$. is complex. Because of $(\nu_{eo}/\omega) << 1$ the real part of the refractive index becomes the familiar expression for an electromagnetic wave in a plasma

$$n_R \approx ck/\omega = (1 - \omega_{pe}^2/\omega^2)^{1/2}$$

The imaginary part of the complex wave vector k describes the damping of wave amplitude due to collisions. Since the intensity I is proportional to the square of the amplitude, we find that the absorption coefficient in the equation

$$I = I_o e^{-\alpha z}$$

becomes

$$\alpha = -2\ \mathrm{Im}(k) = -2(\omega/c)\ n_I$$

From eq (11) also follows, $-2\, n_R n_I = \mathrm{Im}(\varepsilon)$. Thus α can be written

$$\alpha = (\omega/cn_R)\ \mathrm{Im}(\varepsilon)$$

The absorption length $\ell = 1/\alpha$ becomes

$$\ell \approx \frac{c\omega^2}{\omega_{pe}^2 \nu_{eo}} = \frac{3.3 \times 10^{31}}{n_e \lambda^2 \nu_{eo}} \ \mathrm{cm} \qquad (12)$$

where n_e is measured in cm^{-3} and λ in micron.

Since $z/\ell << 1$ the intensity absorbed by the plasma becomes

$$I_o - I \approx I_o(z/\ell) \qquad (13)$$

It is noteworthy from eq (12) and (13) that the absorption of laser energy per electron in a weakly ionized surface layer of depth z is independent of n_e

$$\frac{I_o z}{n_e z \ell} = \frac{I_o \omega_{pe}^2\ \nu_{eo}}{n_e c \omega^2} = \frac{I_o \lambda^2 \nu_{eo}}{3.3 \times 10^{31}} \qquad (14)$$

Consequently, electron heating will occur for any initial electron density present near the surface and it will increase with the desorption of surface layers of absorbed gases (CO_2, H_2O, etc.) because ν_{eo} increases with the build up of the neutral particle density. For atmospheric pressure initially, the laser damage threshold is of the order $15 J/cm^2$ for short pulse Nd radiation. From eq (14) we estimate then that an electron absorbs 5.6eV. Ionization will occur if this energy becomes thermalized between the electrons. The existence of the sheath will enhance the electron-electron collision rate since most of the electrons will be reflected in the sheath and their velocity component v_z goes through zero, thus increasing the Coulomb collision cross section.

For a perfectly reflecting surface the time averaged value of a standing wave shows spatial intensity variations as

$$E^2 = 4E_o^2 \sin^2\left(\frac{2\pi z}{\lambda}\right)$$

with maxima of 4 times increased intensity located at $z = \lambda/4, 3\lambda/4, \ldots$ This higher intensity and the release of neutral particles from the surface should considerably increase the electron heating in the $\lambda/4$ region. Figure 16 shows schematically this influence of the neutral density gradient on the preferential rapid electron heating, ionization and breakdown in a surface layer, near $z = \lambda/4$. The average speed of water molecules released from the surface at 25°C is 592m/s. For $\lambda = 1.06\ \mu m$, the time for desorbed molecules to travel a distance of $\lambda/4$ is thus 0.4 ns. This time will be even shorter as rapid surface heating will occur. This discussion indicates that electrons can gain sufficient energy to ionize neutrals, thus further increasing the electron density and consequently the absorption coefficient. This feedback mechanism will lead to rapid ionization and build up of the local plasma pressure until the arc ignites. Furthermore, laser energy will be preferentially absorbed and less reflected where the arc burns since relative large amounts of material will be ejected from the cathode crater.

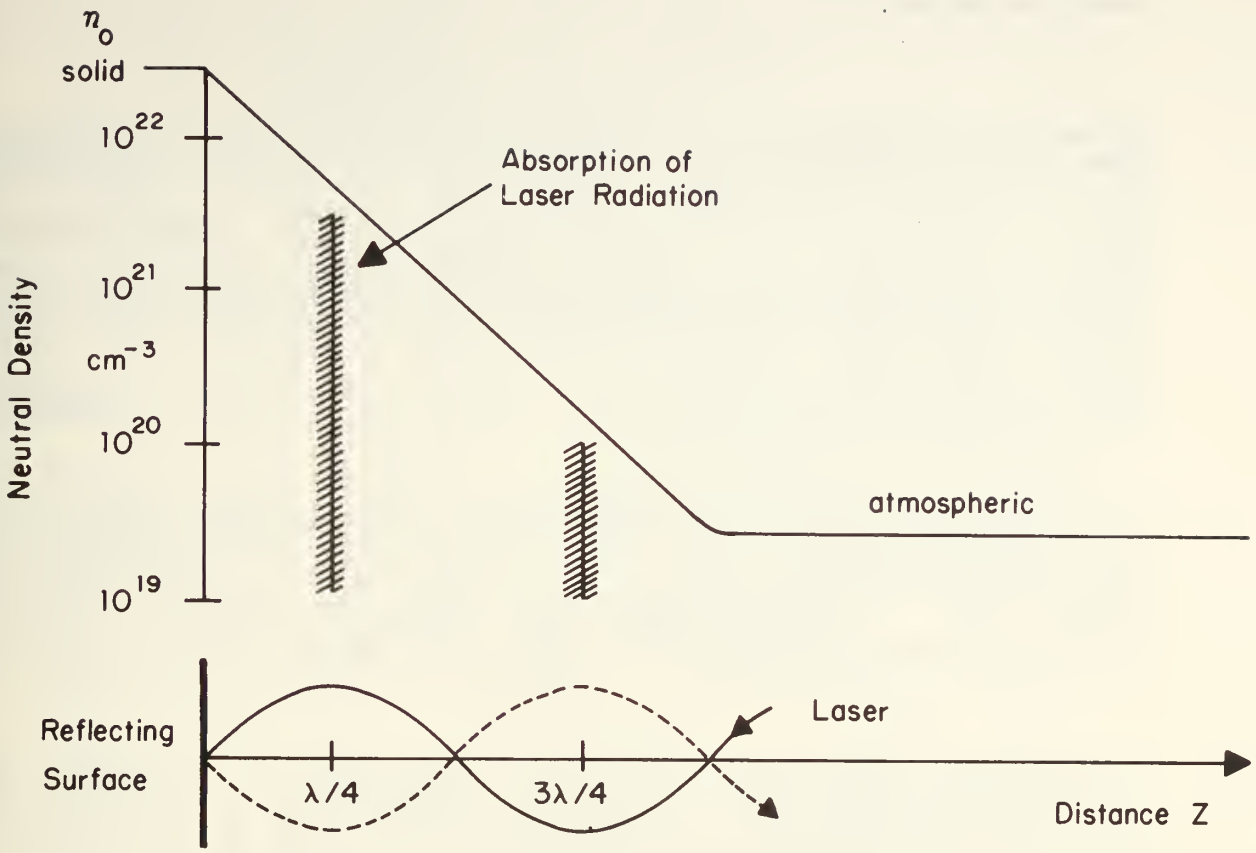

Figure 16. Absorption of short-pulse laser radiation near a reflecting surface. The neutral density gradient in front of the surface is caused by blow-off of surface material.

This contributes to a non-uniform laser energy deposition and plasma build up above the cathode spot until the critical density is reached.

5.3 Unipolar Arcing on "Non-Conducting" Materials

It is apparent that laser-target interaction with its attendant plasma-induced arcing is a dynamic process which must be described in terms of constantly changing variables. Such variables include, but are not limited to, plasma temperature and density, laser power and pulse duration, neutral particle density, absorbed gases, target material and surface preparation, physical properties of the target, like thermal and electrical conductivity and vapor pressure as function of surface temperature. The observed small scale cratering on non-metallic materials indicates that their surfaces exposed to a plasma require sufficient conductivity to provide the electron return current flow to the cathode spot. The modification of the sheath potential due to the radial pressure gradient, eq (7) and (8) provides an r-dependent electron flow from the plasma to the surface ring area $2\pi r\Delta r$

$$i^- = 2\pi r\Delta r n_e(r) e(kT_e/2\pi m)^{1/2} \exp -e[V_p(r)-V_w(r)]/kT_e \qquad (15)$$

where $V_p(r)$ is the plasma potential $V_w(r)$ the potential of the wall and the sheath potential is $V_s(r) = V_p(r)-V_w(r)$. The ion flow to the surface is determined by the number of ions entering the sheath, which corresponds to the ion saturation current [15] and it is independent of the

sheath potential

$$i_s^+ = 0.4\, en_i(r)\, (2kT_e/M_i)^{1/2} 2\pi r\Delta r$$

Differences between i^- and i^+ will charge the surface with a net charge. Since $n_i(r) = n_e(r)$ it is the exponential term in eq (15) which controls the net surface charge density. Electron and ion flows are equal when the sheath potential has the value of the floating potential, $V_s = V_f$. For $V_s(r) < V_f$ we find $i^- > i^+$. Since in accordance with eq (8) the plasma potential decreases with increasing distance r from the the high plasma pressure region above the cathode spot the surface areas $2\pi r\Delta r$ will be charged more negative with increasing r. The r-dependent net surface charge density causes then a surface radial electric field with the electron emitting cathode spot being more positive than the negatively charged surrounding ring areas. Electron surface mobility and diffusion will determine the electron-ion recombination rate on the surface and the electron return current flow to the cathode spot.

The small size observed for craters on silicon and TiC in comparison to the larger size cathode craters for metals may be qualitatively explained by the higher resistivity encountered by the surface electron return current which converges radially inward to the cathode spot. If ohmic heating is assumed to be the primary source for vaporization of material from the cathode spot, a smaller cathode spot diameter is required to achieve sufficient current density. The power dissipated per crater volume V_m is

$$P/V_m = j^2(r)/\sigma_s$$

where σ_s is the surface conductivity of the material. At the cathode spot we must have $j(r) \sim j_{arc}$. Neglecting differences in arc current densities and binding energy, dimensional analysis indicates that the crater size r_o should scale with conductivity roughly as $\sigma_s \propto r_o^2$ which is in qualitative agreement with the experimental observation that lower conductivity material show smaller crater size. In the case of TiC the resistivity is almost two orders of magnitude larger than the one for aluminum. The size of craters observed on TiC is 0.1 to 0.3 μm diameter while for metals the cathode crater is typically 0.7 to 1.5 μm. The actual size would depend also on the burn time of the arc. It is recommended that unipolar arcing on various non-conducting materials be further investigated.

SUMMARY

Unipolar arcing has been shown to be the primary plasma-surface interaction process when a laser produced plasma is in contact with a surface. Evidence of unipolar arcing was found on all targets irradiated at atmospheric pressure that also arced in vacuum, stainless steel, titanium, molybdenum, copper, and aluminum.

Cratering was observed even for a defocused and low-power laser pulse. The minimum laser power density required for the onset of breakdown on the surface is also sufficient to cause arc damage. Never was there a plasma evident without attendant unipolar arc craters. About 500,000 arc craters per cm^2 have been observed on laser illuminated metal surfaces although no external voltage is applied. Smaller size craters with a density of about $10^8/cm^2$ have been found on higher resistivity materials. The higher resistivity requires the radially inward surface return current to converge to a smaller cathode spot size to achieve sufficient power density to vaporize and ionize the material required for running the unipolar arc.

The local increase of the plasma pressure above the cathode spot leads to an electric field configuration which drives the arc current and also facilitates the return current flow to the surface and cathode spot.

Unipolar arcing concentrates the available laser-plasma energy towards the cathode spot. Large scale unipolar arcing on metal surfaces increases the coupling of energy from the laser heated plasma into the target. The ejection of a plasma jet from the cathode crater also causes highly

localized shock waves to propagate into the target, softening it in the process. Thus, material erosion is much more severe than it would be the case for uniform energy deposition over a larger area.

This research has wide spread applications. Any situation in which a sufficiently hot surface plasma exists there will be unipolar micro-arcing. The physics relates to other forms of electrical breakdown on surfaces and electrodes.

ACKNOWLEDGEMENTS

This work was supported by the Naval Postgraduate School Foundation Research Program and in part by the Naval Research Laboratory.

REFERENCES

[1] Robson, A. E. and Thonemann, P. C., Proc. Phys. Soc. 73, 508(1959)
[2) McCracken, G. M., J. Nucl. Mater. 93/94, 3(1980)
[3] Clausing, R. E., Emerson L. C. and Heatherly, L. E., J. Nucl. Mater. 93/94, 150(1980)
[4] McCracken, G. M. and Goodall, D. H. J., Nucl. Fusion 18, 537(1978)
[5] Cohen, S. A., Dylla, H. F., Rossnagel, S. M., Picraux, S. T. and Magee, C. W., J. Nucl. Mater. 76/77, 459(1978)
[6] Staib, P. and Staudemaier, G., J. Nucl. Mater. 76/77, 78(1978)
[7] Schwirzke, F., Oren, L., Talmadage, S., and Taylor, R. J., Phys. Rev. Letters 40, 1181(1978)
[8] Oren, L., Taylor, R. J., and Schwirzke, F., J. Nucl. Mater. 76/77, 412(1978)
[9] Schwirzke, F. and Taylor, R. J., J. Nucl. Mater. 93/94, 780(1980)
[10] Gierke, G. V., Ott, W., and Schwirzke, F., Proc. Fifth International Conference on Ionization Phenomena in Gases, Munich 1961, p. 1412
[11] Schwirzke, F., Beelby, M. H., and Ulrich, H. G., "Basic Mechanisms that Lead to Laser Target Damage", Naval Postgraduate School Report NPS 61-82-002(1981)
[12] Schwirzke, F., Bunshah, R. F., and Taylor, R. J., Thin Solid Films 83(1981)117
[13] Methenv, R. M., An investigation of energy coupling in various arc susceptible and resistant conductors, M.S. Thesis, Naval Postgraduate School, Monterey, California, June 1982
[14] Jenkins, W. F., and Schmidt, W. R., Thermal coupling and damage mechanisms of 1.06 micron laser radiation and laser produced plasma on selected materials, M.S. Thesis, Naval Postgraduate School, December 1982
[15] Schwirzke, F., Phys. Fluids, 9, 2244(1966)

DISTRIBUTION LIST

1.	Professor Fred Schwirzke Code 61Sw Naval Postgraduate School Monterey, CA 93940	64
2.	Dudley Knox Library Naval Postgraduate School Monterey, CA 93940	2
3.	Naval Research Laboratory Washington, DC 20375	2
4.	Defense Technical Information Center ATTN: DTIC-DDR Cameron Station Alexandria, VA 22314	2

DUDLEY KNOX LIBRARY
3 2768 00343086 9